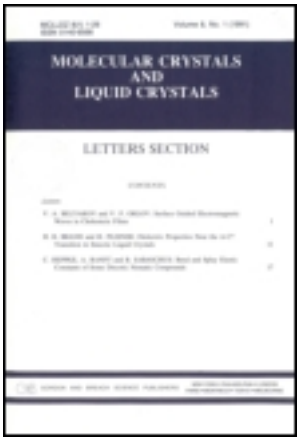

Molecular Crystals and Liquid Crystals
Publication details, including instructions for authors and subscription information:
http://www.tandfonline.com/loi/gmcl20

Characterization of Hydrogen Bonded Liquid Crystals Formed by Suberic Acid and Alkyl Benzoic Acids

R. Rajanandkumar [a], N. Pongali Sathya Prabu [a] & M. L. N. Madhu Mohan [a]
[a] Liquid Crystal Research Laboratory (LCRL), Bannari Amman Institute of Technology, Sathyamangalam, 638 401, Tamil Nadu, India
Published online: 16 Dec 2013.

To cite this article: R. Rajanandkumar, N. Pongali Sathya Prabu & M. L. N. Madhu Mohan (2013) Characterization of Hydrogen Bonded Liquid Crystals Formed by Suberic Acid and Alkyl Benzoic Acids, Molecular Crystals and Liquid Crystals, 587:1, 60-79, DOI: 10.1080/15421406.2013.821383

To link to this article: http://dx.doi.org/10.1080/15421406.2013.821383

Mol. Cryst. Liq. Cryst., Vol. 587: pp. 60–79, 2013

ISSN: 1542-1406 print/1563-5287 online
DOI: 10.1080/15421406.2013.821383

Taylor & Francis
Taylor & Francis Group

Characterization of Hydrogen Bonded Liquid Crystals Formed by Suberic Acid and Alkyl Benzoic Acids

R. RAJANANDKUMAR, N. PONGALI SATHYA PRABU, AND M. L. N. MADHU MOHAN*

Liquid Crystal Research Laboratory (LCRL), Bannari Amman Institute of Technology, Sathyamangalam 638 401, Tamil Nadu, India

An inter hydrogen bonded homologous series with seven liquid crystalline complexes has been isolated and characterized. Double complementary hydrogen bonds are formed between a nonmesogen suberic acid (SA) and mesogenic p-n-alkyl benzoic acid (nBA); the series is referred as SA + nBA. Hydrogen bond is evinced by FTIR studies, while the mesogenic phases are identified by polarizing optical microscopic studies that are further substantiated by differential scanning calorimetry. Phase diagram is composed of nematic, smectic C, smectic F, and smectic G phases. The variation of tilt angle of various homologues with temperature in smectic C is fitted to a power law and the exponent value (β) is found to be in agreement with mean field predicted value (0.5). Orders of the various phase transitions are established by Cox method. Dielectric studies enable to identify phases and evaluate relaxation processes in smectic C and the corresponding activation energy is derived from the data.

Keywords Cox ratio; dielectric spectrum; hydrogen bonded liquid crystals; mean field theory; order of phase transition

1. Introduction

Applicational aspect of liquid crystals made the global researchers to design [1–4], synthesize [5,6], characterize [7,8], and develop new mesogenic materials [9–12]. In the past two decades, hydrogen bonded liquid crystals (HBLC) earn overwhelming interest among several working groups [13–19] due to their molecular reorganization and self-assembly capability. These HBLC are designed and synthesized from materials selected on the basis of their applicational aspects [20–22] and commercial viabilities [23,24]. Hydrogen bond enables various mesogenic [25–28] and nonmesogenic [29–31] compounds to form complexes that exhibit rich phase polymorphism. Phases like nematic, smectic C are of great importance because of their commercial viability.

Weak noncovalent hydrogen bonding existing between the chemical moieties paved way for the formation of supramolecular hydrogen bonded liquid crystal mesogens. Literature survey indicates that Paleos [1,2] and Kato [18,19] synthesized a variety of liquid crystals induced by this intermolecular hydrogen bonding between pyridyl moieties. Many

*Address correspondence to M. L. N. Madhu Mohan, Liquid Crystal Research Laboratory (LCRL), Bannari Amman Institute of Technology, Sathyamangalam 638 401, Tamil Nadu, India. Tel.: +91 9442437480; Fax: +91 4295 223 775. E-mail: mln.madhu@gmail.com

such supramolecular hydrogen bonded liquid crystal systems like molecular liquid crystals [32,33], polymer liquid crystals [34,35], and ferroelectric liquid crystals [36–38] have been investigated. Single bond [39–41], double bond [42], and multiple bond [43,44] HBLC are also synthesized and reported. Numerous techniques such as electrical [45], optical [46], and thermal techniques [47–49] are used in measuring the physical parameters of the mesogens.

With our previous experience in designing [25–28] and synthesizing [40–42] liquid crystals and in continuation of our efforts to understand hydrogen bonded mesogens in the present work, a successful attempt has been made to design and isolate a homologous series of HBLC. The mesogenic *p*-*n*-alkyl benzoic acids (*n*BA; where *n* represents the alkyl carbon number from 2 to 8) formed linear complementary hydrogen bonds with suberic acid (SA). Phase thermal range, thermal stability factor of various phases, tilt angle, dielectric relaxations, and their corresponding activation energy are also discussed.

2. Experimental

Optical textural analyses were observed using Nikon polarizing microscope equipped with Nikon digital CCD camera system with 5 megapixels and 2560 × 1920 pixel resolution. The liquid crystalline texture were processed, analyzed, and recorded with the aid of NIS imaging software system. The temperature control of liquid-crystal cell was equipped with Instec HCS402-STC 200 temperature controller (Instec) to a temperature resolution of ±0.1°C. This unit was interfaced with computer by IEEE-STC 200 to control and monitor the temperature. The liquid crystal sample was filled by capillary action in its isotropic state into a commercially available (Instec) polyamide-buffed cell with 4 μm spacer. The transition temperature and corresponding enthalpy values were obtained by differential scanning calorimetry (DSC; Shimadzu DSC-60). Fourier transform infrared (FTIR) spectra were recorded (ABB FTIR MB3000) and analyzed with MB3000 software. Dielectric studies were performed using HP 4192A impedance analyzer. The *n*BA and SA were supplied by Sigma Aldrich (Germany) and all solvents used were high-performance liquid chromatography (HPLC) grade.

2.1. Synthesis of HBLC

All the intermolecular complementary hydrogen bonded compounds are prepared by mixing two moles of *n*BA with one mole of SA in DMF. Further, they are subjected to constant stirring for 12 h at ambient temperature (30°C) until a white precipitate in a dense solution is formed. Excess DMF is dried and the sample is recrystallized. The molecular structure of present homologous series is depicted in Fig. 1 while the synthetic route is depicted as

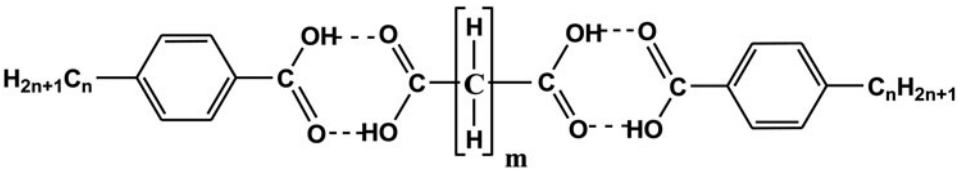

Figure 1. Molecular structure of SA + *n*BA homologous series.

Scheme 1, where *n* represents the alkyl carbon number and *m* is number of H–C–H spacer groups.

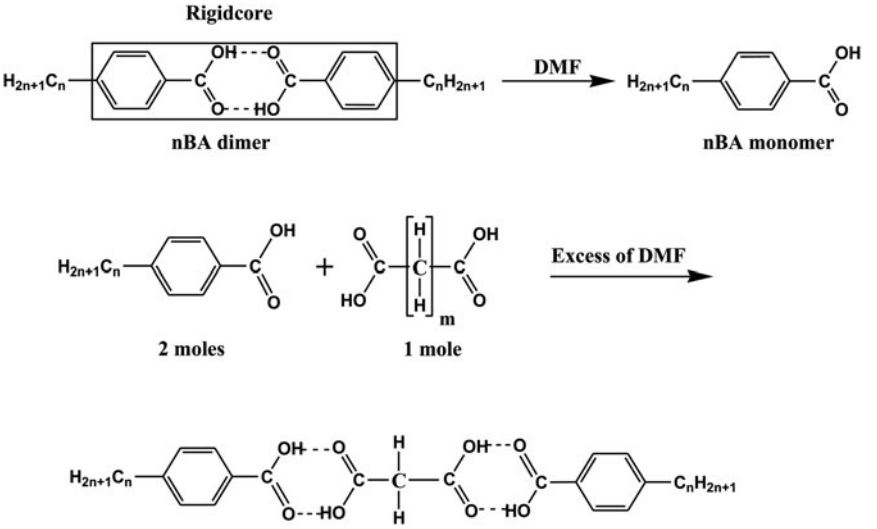

Scheme 1. Scheme representing the formation of SA + *n*BA hydrogen bonded series.

3. Results and Discussion

All the mesogens synthesized are insoluble in water and sparingly soluble in common organic solvents such as methanol, ethanol, benzene, and dichloro methane. However, they show high degree of solubility in coordinating solvents like DMSO and pyridine. They melt at specific temperatures below 116.5°C (Table 1). Further, all these mesogens show high thermal and chemical stability when treated with repeated thermal scans during polarizing optical microscope and DSC studies.

3.1. Phase Identification

The observed phase variance, transition temperatures, and corresponding enthalpy values obtained by DSC in the cooling and heating cycles for the SA + *n*BA complexes are presented in Table 1. The transition temperatures and phases observed are in concurrence with POM data.

3.1.1. Phase Variance of SA + nBA Homologous Series. Phase transition temperatures and enthalpy values of SA + *n*BA homologous series are tabulated in Table 1. SA with *n*BA (where $n = 2$–8) designated as SA + *n*BA homologous series is found to exhibit characteristic textures [50], viz., nematic (N) (droplet texture, Plate 1), smectic C (schlieren texture, Plate 2), smectic F (chequered board texture, Plate 3), and smectic G (smooth multicolored mosaic texture, Plate 4), respectively. The general phase sequence of various homologues of SA + *n*BA in cooling and heating runs can be shown as:

$$\text{Isotropic} \rightleftharpoons \text{N} \rightarrow \text{Sm C} \rightleftharpoons \text{Crystal (SA + 8BA)}$$

$$\text{Isotropic} \rightleftharpoons \text{Sm C} \rightarrow \text{Sm G} \rightleftharpoons \text{Crystal (SA + 7BA)}$$

Table 1. Transition temperatures obtained by different techniques for SA + *n*BA homologous series. Enthalpy values (J g^{-1}) are given in parenthesis

Complex	Phase variance	Study	Crystal to melt	N	C	F	G	Crystal
SA + 8BA	NC	DSC (h)	92.6 (30.67)	102.7 (7.25)	#			
		DSC (c)		104.8 (2.45)	100.6 (7.43)			86.1 (24.07)
		POM (c)		105.2	100.9			86.2
SA + 7BA	CG	DSC (h)	94.4 (43.66)		106.1 (11.81)		#	
		DSC (c)			105.1 (6.8)		98 (45.01)	86.5 (35.61)
		POM (c)			105.6		98.4	86.3
SA + 6BA	CF	DSC (h)	90.8 (42.33)		#	102.5 (8.75)		
		DSC (c)			117.2 (5.76)	96 (45.55)		81.0 (39.78)
		POM (c)			117.6	96.3		81.1
SA + 5BA	CF	DSC (h)	79.5 (35.97)		#	#		
		DSC (c)			119.1 (3.00)	97.5 (61.89)		71.3 (36.43)
		POM (c)			119.6	97.9		71.5
SA + 4BA	NCF	DSC (h)	91.8 (40.16)	115.8 (3.87)	100.1 (7.78)	#		
		DSC (c)		109.7 (3.89)	98.3 (4.19)	94.4 (4.50)		79.5 (39.91)
		POM (c)		110.1	98.6	94.6		79.6
SA + 3BA	FG	DSC (h)	116.5 (127.15)			#	#	
		DSC (c)				113.2 (3.41)	108.7 (6.89)	101.4 (83.81)
		POM (c)				113.6	108.9	101.5
SA + 2BA	F	DSC (h)	100.5 (78.81)			114.9 (1.57)		
		DSC (c)				113.2 (3.28)		88.2 (102.13)
		POM (c)				113.4		88.3

Note. (h), heating run; (c), Cooling run; #, monotropic transition in heating run. Enthalpy values in J g^{-1}.

$$\text{Isotropic} \rightarrow \text{Sm C} \rightleftharpoons \text{Sm F} \rightleftharpoons \text{Crystal (SA} + 6\text{BA)}$$

$$\text{Isotropic} \rightarrow \text{Sm C} \rightarrow \text{Sm F} \rightleftharpoons \text{Crystal (SA} + 5\text{BA)}$$

$$\text{Isotropic} \rightleftharpoons \text{N} \rightleftharpoons \text{Sm C} \rightarrow \text{Sm F} \rightleftharpoons \text{Crystal (SA} + 4\text{BA)}$$

$$\text{Isotropic} \rightarrow \text{Sm F} \rightarrow \text{Sm G} \rightleftharpoons \text{Crystal (SA} + 3\text{BA)}$$

$$\text{Isotropic} \rightleftharpoons \text{Sm F} \rightleftharpoons \text{Crystal (SA} + 2\text{BA)}$$

Monotropic and enantiotropic transitions are depicted as single and double arrows respectively.

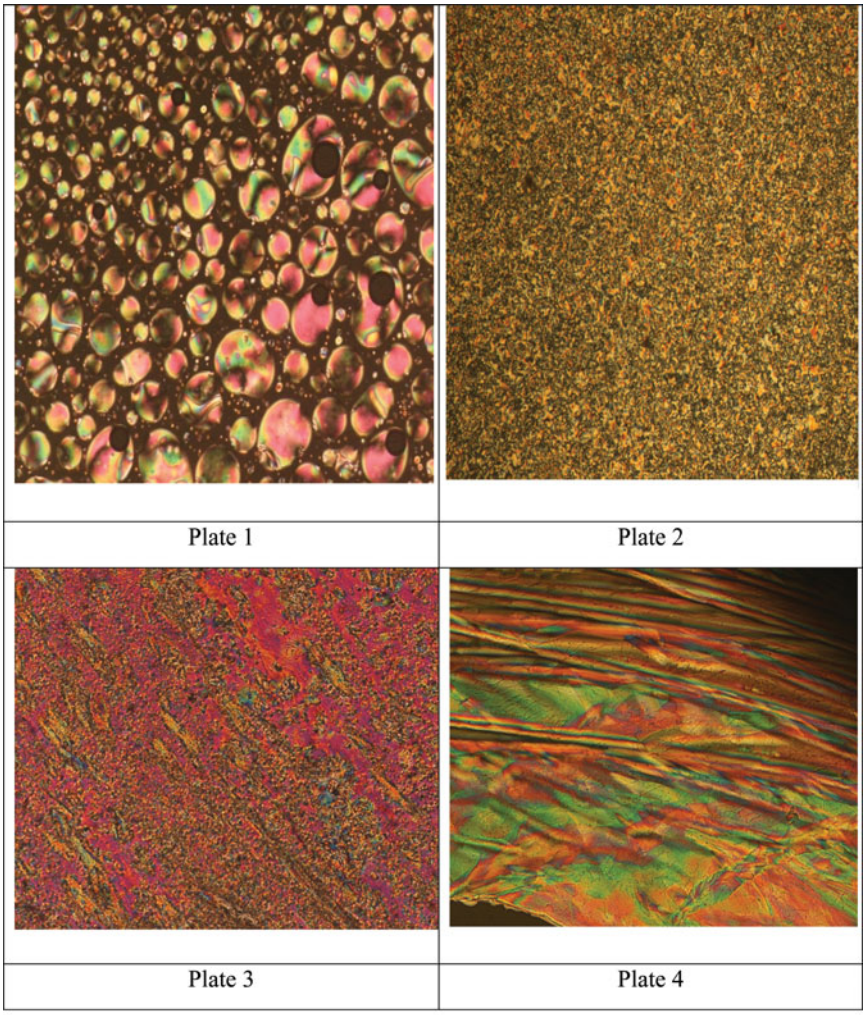

Plate 1. Nematic droplet texture observed in SA + 8BA.
Plate 2. Schlieren smectic C texture observed in SA + 7BA.
Plate 3. Chequered board texture of smectic F observed in SA + 2BA.
Plate 4. Smooth multicolored mosaic texture of smectic G observed in SA + 3BA.

Table 2. FTIR peak assignments for precursors and SA + *n*BA series

Complex	$(OH)_{acid}$	$(CO)_{acid}$	Precursor	$(OH)_{acid}$	$(CO)_{acid}$
SA + 8BA	2926	1689	8BA	2924	1682
SA + 7BA	2933	1693	7BA	2927	1682
SA + 6BA	2936	1695	6BA	2927	1687
SA + 5BA	2930	1693	5BA	2927	1686
SA + 4BA	2955	1695	3BA	2927	1686
SA + 3BA	2960	1689	4BA	2959	1681
SA + 2BA	2946	1690	2BA	2962	1687

3.2. Fourier Transform Infrared Spectroscopy

IR spectra for all the seven homologues of SA + *n*BA series have been recorded in the solid state (KBr) at room temperature. FTIR data of all the homologues are tabulated in Table 2. As a representative case, FTIR spectrum of SA + 3BA complex is shown in Fig. 2 and is discussed elaborately. It is reported [51,52] that in the alkyloxy benzoic acids, carboxylic acid exists in monomeric form and the stretching vibration of C=O is observed at 1760 cm^{-1}. Further it is known [51] that when a hydrogen bond is formed between carboxylic acids, it results in lowering of the carbonyl frequency that has been detected in the present hydrogen bonded complexes. A noteworthy feature in the spectrum of the SA + 3BA is the appearance of sharp peak at 1689 cm^{-1}, which clearly suggests the dimer formation, in particular the carbonyl group vibration [53–55]. A carboxylic acid existing in monomeric form in dilute solution absorbs at about 1760 cm^{-1} because of the electron withdrawing effect. However, acids in concentration solution or in solid state tend to dimerize through hydrogen bonding. It is reported [52] that this dimerization weakens the C=O bond and lowers the stretching force constant K, resulting in a lowering of the carbonyl frequency of saturated acids to ~1710 cm^{-1}. This result concurs with the reported data of Kato *et al*. [51]. Hence, in the present complexes the formation of H bonding

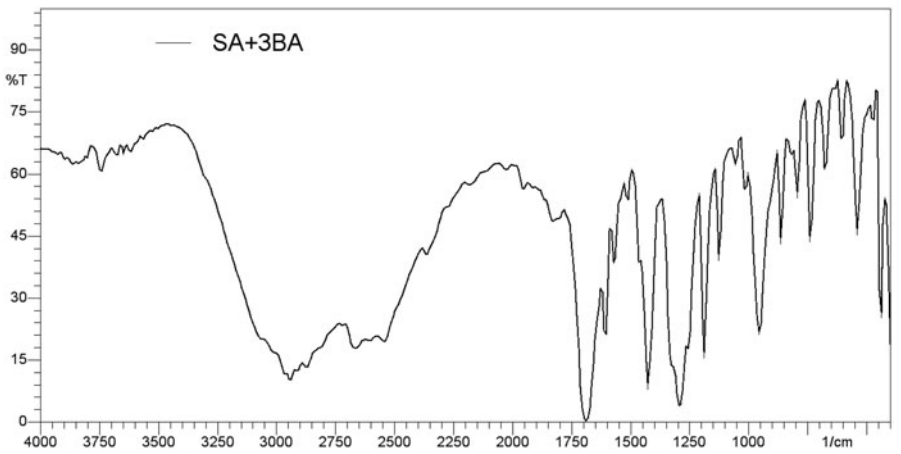

Figure 2. FTIR spectra of SA + 3BA complex.

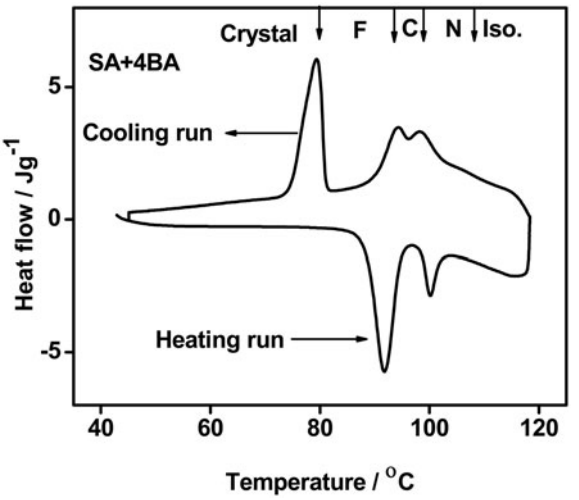

Figure 3. DSC thermogram of SA + 4BA complex.

is established by FTIR. A similar trend of result is followed in all the other synthesized hydrogen bonded complexes.

3.3. DSC Studies

DSC thermograms are obtained in heating and cooling cycles of the sample. The sample is crimped in an aluminum pan and heated at a scan rate of 10°C min^{-1} in nitrogen environment and held at its isotropic temperature for 1 min to attain thermal stability. The cooling run is also performed with the same scan rate of 10°C min^{-1}. A program is written in the DSC software TA 60 specifying the scan rate, hold temperature, and hold time. Respective equilibrium transition temperature and corresponding enthalpy values for each of the mesogens are recorded using the software of the DSC. DSC results are in conformity with the POM data. As a representative case, DSC thermogram obtained for SA and butyl benzoic acid, SA + 4BA, complex depicted in Fig. 3 is discussed. From Fig. 3 and Table 1, it can be inferred that in the DSC the heating run exhibits three endothermic peaks at 91.8°C, 115.8°C, and 100.1°C with enthalpy values of 40.16 J g^{-1}, 3.87 J g^{-1}, and 7.78 J g^{-1}, respectively. These three peaks correspond to the crystal to melt, melt to nematic, and nematic to smectic C phase transitions. The cooling run exhibits four peaks at 109.7°C, 98.3°C, 94.4°C, and 79.5°C with enthalpy values of 3.89 J g^{-1}, 4.19 J g^{-1}, 4.50 J g^{-1}, and 39.91 J g^{-1}, respectively. These exothermic peaks correspond to isotropic to nematic, nematic to smectic C, smectic C to smectic F, and smectic F to crystal phases, respectively. Thus, all the transitions are enantiotropic in cooling run while in the heating run smectic F to smectic C is observed to be monotropic.

3.4. Phase Variance of Precursors and SA + nBA

SA and alkyl benzoic acid are the precursors of the present homologues series. SA is nonmesogenic while alkyl benzoic acid is reported [56] to exhibit nematic and smectic G phases. The present homologues series of SA + *n*BA exhibit nematic, smectic C, smectic F, and smectic G phases, respectively.

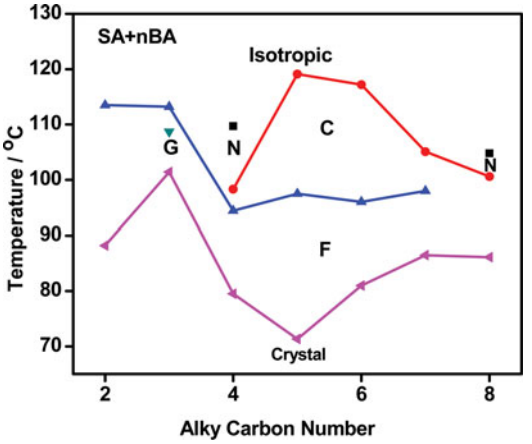

Figure 4. Phase diagram of SA + *n*BA homologous series.

3.4.1. Phase Diagram of SA + nBA. Figure 4 illustrates the phase diagram of SA + *n*BA homologous series. Following points can be elucidated from the phase diagram.

(1) Phase diagram comprises of four phases namely, nematic, smectic C, smectic F, and smectic G.
(2) The thermal spans of various phases in descending order are smectic F, smectic C, nematic, and smectic G.
(3) The lower homologues, i.e., SA + 2BA and SA + 3BA, exhibit higher-ordered phases viz., smectic F and smectic G.
(4) Interestingly, nematic is observed only in two complexes viz., SA + 4BA and SA + 8BA.
(5) Smectic F is quenched by smectic C in SA + 4BA to SA + 8BA complexes.
(6) Maximum mesogenic range is observed in SA + 5BA, while minimum mesogenic range is observed in SA + 3BA (Fig. 5).
(7) In the even complexes namely, SA + 2BA, SA + 4BA, and SA + 8BA, the isotropic temperatures are gradually reduced. Only exception to this trend is SA + 6BA.
(8) Phases have been periodically induced in this series. Smectic F is observed in SA + 2BA, smectic G is induced in SA + 3BA, while nematic and smectic C are induced in SA + 4BA. Thus, with the increment of alkyl carbon number, inducement of phases is clearly noticed

3.5. Thermal Stability Factor

It is reported [57,58] that when the liquid crystal molecules have two end chains, the phase transition temperatures are higher for the systems with equal chain length (symmetric). In a symmetric system, the end chains affect the phase transition temperatures as well as the temperature ranges of various phases. The molecular weights of terminal chain could be considered as the measure of balancing and if they are nearly equal, the system is balanced. In other words, the system is symmetric about its molecular short axis.

Phase stability is one of the important parameters that govern the utility of the mesogen. Phase stability of nematic is discussed. The term nematic phase stability can be attributed to isotropic to nematic transition temperature as well as to the temperature range of nematic phase. It is reasonable to consider both the above factors and define a parameter called stability factor (S). The stability factor for nematic, S_N, is given by

$$S_N = T_{mid} {}^* \Delta T_N,$$

where, T_{mid} is the mid nematic temperature and ΔT_N, the nematic thermal range. In this manner, the thermal stability of smectic C, smectic F, and smectic G exhibited by different homologues are calculated and tabulated in Table 3. From Table 3, it can be seen that in general, in all the phases, the stability is decreased with increase in carbon number.

3.5.1. Estimation of Order of Transition: Cox Parameter. Many theories such as Landau theory and mean field theory [59] deal with the order of the phase transitions possessed by the material. A phase transition is noted by a continuous or discontinuous change in the equilibrium value of the order parameter when the system transforms from one phase to the other. It is said to be the first-order transition when it is discontinuous and if the state is continuous it is assigned to be second-order transition. Thus, the theoretical description of

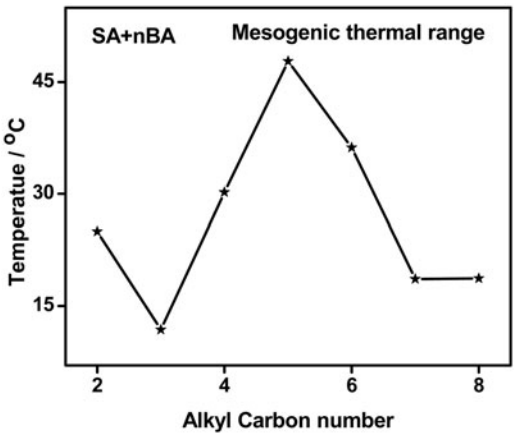

Figure 5. Mesogenic thermal range exhibited by SA + *n*BA homologous series.

Table 3. Thermal stability factor obtained for various phases of SA + *n*BA complexes

Complex	N	C	F	G
SA + 2BA	—	—	2517.5	—
SA + 3BA	—	—	499.27	766.86
SA + 4BA	1185.6	375.76	1295.55	—
SA + 5BA	—	2339.28	2211.28	—
SA + 6BA	—	2259.92	1327.5	—
SA + 7BA	—	721.00	—	1060.87
SA + 8BA	431.34	1353.57	—	—

a phase transition is equivalent to the determination of the free energy density as a function of the order parameter, its spatial derivatives, and the temperature.

Navard and Cox [47] reported a new experimental method in determining the order of phase transition, in which either the scan rate (either endothermic or exothermic) or the weight of the sample can be a varying parameter with respect to the phase transition peak height obtained by DSC thermograms. According to Cox theory [47], the first- and second-order transitions can be classified basing on the ratio (N_x) of the measured phase transition peak heights. The ratio (N_x) is $1 < N_C \geq \sqrt{2}$ for an isothermal first-order transition and $N_C = 2$ for a second-order transition. The magnitude nearing 1.8 and above can be considered as weak first-order transition. The N_x ratio of the individual phases is calculated as discussed below.

DSC thermograms of the mesogens are recorded at programmed scan rate in heating and cooling cycles. The mesogen is heated with a scan rate of 5°C min^{-1} and held at its isotropic temperature for 1 min so as to attain thermal stability. The process is repeated for a scan rate of 10°C min^{-1}. The individual cooling runs are also performed with 10°C min^{-1} and 5°C min^{-1} scan rates. The peak height of the individual phases exhibited by the corresponding mesogens both in cooling and heating cycles of two different scan rates are measured and the ratio of the peaks with scan rates of 10°C min^{-1} and 5°C min^{-1} are referred as Cox ratio N_x.

For the entire series, DSC thermograms with scan rates of 10°C min^{-1} and 5°C min^{-1} are recorded. The magnitude of the N_x ratio and their corresponding order of the transition are tabulated in Table 4. Thus, the order of the phase transition has been established by qualitative treatment.

3.6. Optical Tilt Angle Studies

The optical tilt angle is deduced by optical extinction method [60] in smectic C phase for all the members of SA + *n*BA homologous series. Figure 6 depicts such variation of optical tilt angle with temperature for SA + *n*BA (where $n = 2$–8) series. The theoretical

Table 4. Phase transition order estimation by Cox method

Complex	Phase	Ratio	Order of transition
SA + 8BA	N	0.99	First order
	C	0.97	First order
SA + 7BA	C	1.46	First order
	G	1.57	First order
SA + 6BA	C	1.91	Weak first order
	F	1.80	Weak first order
SA + 5BA	C	1.68	First order
	F	1.66	First order
SA + 4BA	N	1.63	First order
	C	2.50	Second order
	F	2.39	Second order
SA + 3BA	F	1.52	First order
	G	1.69	First order
SA + 2BA	F	1.54	First order

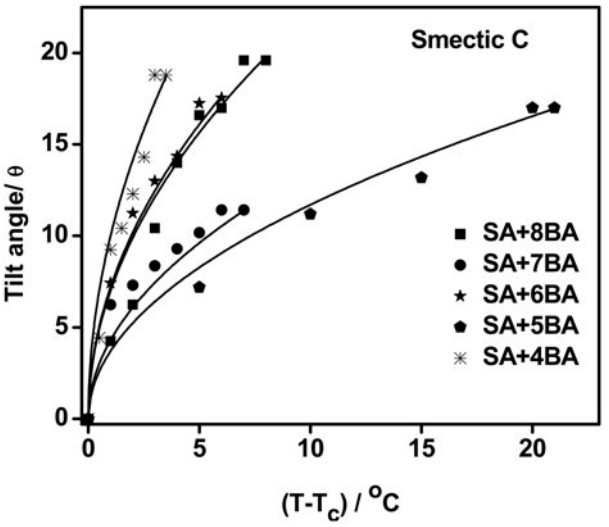

Figure 6. Temperature variation of tilt angle in smectic C phase of SA + *n*BA series.

fit obtained is denoted by the solid line. Further, the tilt angle increases with decreasing temperature. For complexes SA + 8BA, SA + 7BA, SA + 6BA, SA + 5BA, and SA + 4BA, the maximum magnitudes of tilt angle are observed to be 19°6′, 18°24′, 17°54′, 18°6′, and 18°36′, respectively. These large magnitudes of the tilt angle are owed to the direction of the soft covalent hydrogen bond interaction that spreads along molecular long axis with finite inclination. Tilt angle is a primary-order parameter [61] and the temperature variation is estimated by fitting the observed data of θ (T) to the relation:

$$\theta(T)\alpha(T_C - T)^{\beta} \tag{1}$$

The critical exponent β value estimated by fitting the data of θ (T) to the above Equation (1) is found to be 0.50 to agree with the mean field prediction [59,62].

3.7. Dielectric Relaxations

Dielectric dispersion, i.e., frequency variation of dielectric loss exhibited by SA + 4BA, SA + 5BA, SA + 7BA, and SA + 8BA, are studied at different temperatures in smectic C phase in the frequency range of 5 Hz to 13 MHz. An impedance analyzer (Agilent 4192A LF) is operated with $1V_{P\text{-}P}$ oscillating signal with zero bias field. Relative permittivity ε'_r (ω) and dielectric loss ε'' (ω) are calculated by the following equations:

$$*\varepsilon'_r(\omega) = \varepsilon'_r(\omega) - j\varepsilon''(\omega)$$
$$\varepsilon'_r(\omega) = [C_{LC} - C_{leads}]/[C_{empty} - C_{leads}]$$
$$*\varepsilon'_r(\omega) = \tan\delta(\omega)^*\varepsilon_r(\omega)$$

To detect the possible relaxation in the SA + *n*BA complexes, the mesogens are scanned in the frequency range of 5 Hz to 13 MHz at different temperatures in the smectic C phase of the corresponding complex. The relaxation frequency (f_r) increases with lowering temperature, which is suggestive of an Arrhenius behavior [63–65] as it reflects the collective

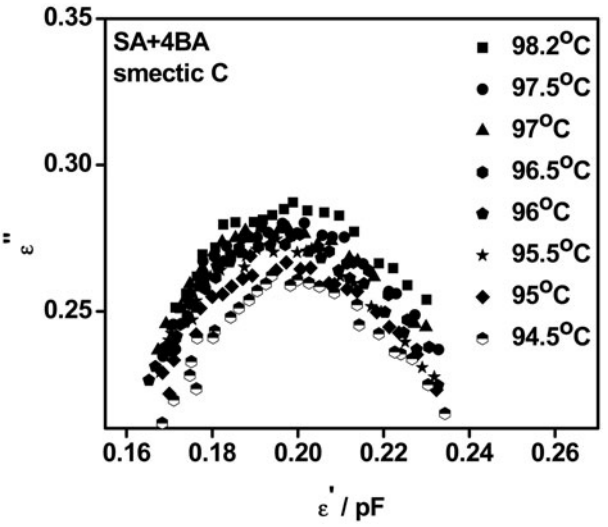

Figure 7. Dielectric dispersion curves in smectic C phase of SA + 4BA complex.

response. Further, the magnitude of the dielectric loss is shifted and is not suppressed by the temperature. The slope of the log of relaxation frequency to inverse of temperature, referred as Arrhenius plot, gives the activation energy of the phase.

The corresponding dispersion curves and Arrhenius plots for all the complexes studied are illustrated in Figs. 7–12 and they appear to be asymmetric about $\varepsilon''_{\max}$. Such a asymmetric non-Debbie's type of off-centered dispersion is studied by Cole-Davidson theory given by

$$\varepsilon''(\omega) = \{\varepsilon_\infty - [(\Delta\varepsilon)]/[1 + (j\omega\tau)^{1-\alpha}]\},$$

where

$\Delta\varepsilon = (\varepsilon_{o\text{-}}\ \varepsilon_\infty) =$ the dielectric increment (strength)

$\omega = 2\pi f$ (where f is the frequency of AC signal)

$\omega =$ relaxation time, i.e., $1/f_r$

$\alpha =$ the distribution parameter (or degrees of freedom) to estimate the influence of environment of dipoles and its fixation in the molecular frame during the reorientation to the field.

3.7.1. Dielectric Relaxations in SA + 4BA. The dielectric relaxations in SA + 4BA complex have been investigated in the entire thermal span of smectic C phase (98.2°C–94.5°C) at eight temperatures, viz., 98.2°C, 97.5°C, 97°C, 96.5°C, 96°C, 95.5°C, 95°C, and 94.5°C, respectively.

The shift of the relaxation frequency to higher side with decrease in temperature can be noticed from Fig. 7. The relaxation frequency at 98.2°C is 180 KHz with a ε'' value of 0.2872; it has shifted to 230 KHz as the temperature has decreased to 94.5°C with a ε'' value of 0.2622. Thus, in this complex the relaxation frequency in smectic C phase is inversely proportional to the temperature. The distribution parameter α has been calculated for each relaxation process. The magnitude of α decreased with increment in temperature. The value of distribution parameter α is 0.4884 at 98.2°C while it increased to 0.8026 at

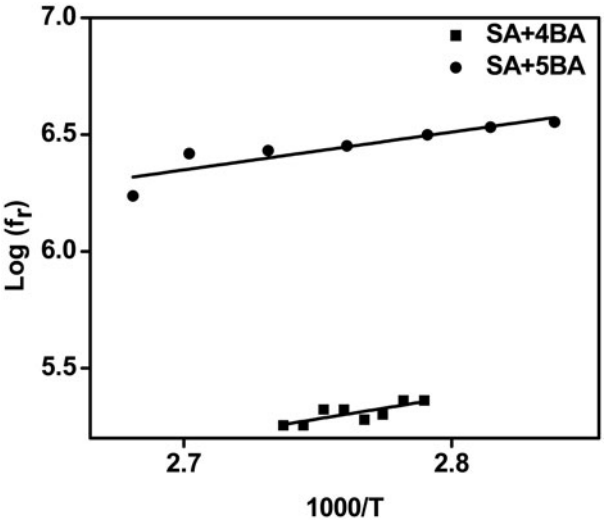

Figure 8. Arrhenius plot of SA + 4BA and SA + 5BA complexes.

94.5°C. From the above data plots, Arrhenius plot (Fig. 8) is constructed and the activation energy is estimated to be 1.8589 eV. The values of relaxation frequency and corresponding temperature and activation energy are listed in Table 5.

3.7.2. Relaxations in SA + 5BA. The dielectric relaxations in SA + 5BA complex is studied covering the entire thermal span of smectic C phase (119°C–101°C) at seven temperatures, viz., 119°C, 116°C, 113°C, 110°C, 107°C, 104°C, and 101°C, respectively. The corresponding dispersion curves are illustrated in Fig. 9.

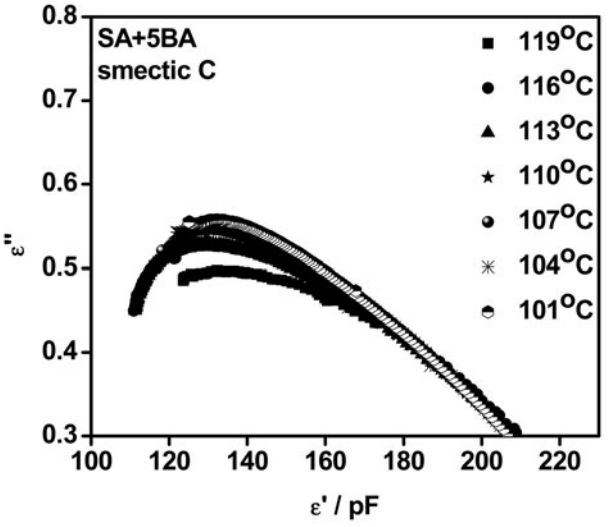

Figure 9. Dielectric dispersion curves in smectic C phase of SA + 5BA complex.

Table 5. Values of relaxation frequency and corresponding temperature along with activation energy for SA + *n*BA ($n = 4,5,7$ and 8) complexes in smectic C phase

Complex	T (°C)	Frequency (KHz)	ε''_{max}	α (rad)	Activation energy (eV)
SA + 8BA	98.1	825	0.3888	0.4711	2.0988
	97.1	800	0.3905	0.5235	
	96.1	775	0.3855	0.5933	
	95.1	1525	0.4054	0.6631	
	94.1	1125	0.354	0.698	
	93.2	1050	0.3409	0.7329	
	92.2	1050	0.3428	0.7503	
	91.2	1200	0.3441	0.7678	
	89.2	1050	0.3453	0.8027	
SA + 7BA	105	575	0.4408	0.4188	0.9554
	104.5	575	0.4338	0.4886	
	104	625	0.4306	0.5060	
	103.5	625	0.4309	0.5758	
	103	650	0.43	0.5933	
	102.5	650	0.4297	0.6107	
	102	650	0.4299	0.6612	
	101.5	625	0.4298	0.698	
SA + 5BA	119	1725	0.4976	0.2965	1.6188
	116	2625	0.5277	0.3488	
	113	2700	0.5265	0.4012	
	110	2825	0.5323	0.4186	
	107	3150	0.5468	0.4710	
	104	3400	0.5543	0.5233	
	101	3575	0.5574	0.6105	
SA + 4BA	98.2	180	0.2872	0.4884	1.8589
	97.5	180	0.2802	0.5233	
	97	210	0.2787	0.5756	
	96.5	210	0.279	0.6105	
	96	190	0.2757	0.6280	
	95.5	200	0.2747	0.6628	
	95	230	0.2689	0.7326	
	94.5	230	0.2622	0.8026	

In this complex, the magnitude of dielectric loss increases with decrement of temperature. The relaxation frequency is noted as 1725 KHz at 119°C with a ε'' value of 0.4976. Further frequency is shifted to 3575 KHz as the temperature is decreased to 101°C with a ε'' value of 0.5574. Thus, the relaxation frequency is inversely proportional to the temperature in this phase.

The distribution parameter α has been calculated for each relaxation process. The magnitude of α increases with decrease in temperature. The value of distribution parameter α is 0.2965 at 119°C while it increased to 0.6105 at 101°C. From the above data plots, Arrhenius plot (Fig. 8) is constructed and the activation energy is estimated to be 1.6188 eV.

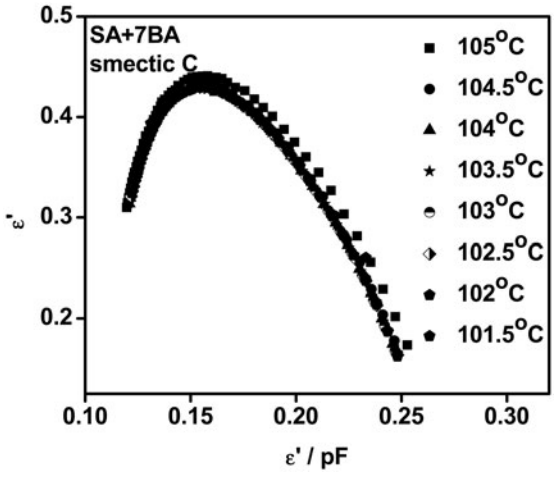

Figure 10. Dielectric dispersion curves in smectic C phase of SA + 7BA complex.

The values of relaxation frequency and corresponding temperature and activation energy are listed in Table 5.

3.7.3. Relaxations in SA + 7BA. The dielectric relaxations for SA + 7BA complex have been studied in the entire thermal span of smectic C phase (105°C to 101.5°C) at eight temperatures, viz., 105°C, 104.5°C, 104°C, 103.5°C, 103°C, 102.5°C, 102°C, and 101.5°C, respectively. The corresponding dispersion curves are illustrated in Fig. 10, which are classified as Cole-Davidson relaxation process.

In this complex, the magnitude of dielectric loss increases with increment in temperature. The relaxation frequency is noted as 575 KHz at 105°C with a ε'' value of 0.4408. Further frequency is shifted to 625 KHz as the temperature is decreased to 101.5°C with a ε'' value of 0.4298. Thus, the relaxation frequency is inversely proportional to the temperature in this phase.

The distribution parameter α has been calculated for each relaxation process. The magnitude of α increases with decrease in temperature. The value of distribution parameter α is 0.4188 at 105°C while it increased to 0.698 at 101.5°C. From the above data plots, Arrhenius plot (Fig. 11) is constructed and the activation energy is estimated to be 0.9554 eV. The values of relaxation frequency and corresponding temperature and activation energy are listed in Table 5.

3.7.4. Relaxations in SA + 8BA. The dielectric relaxations in SA + 8BA complex have been investigated in the entire thermal span of phase (98.1°C–89.2°C) at nine temperatures, viz., 98.1°C, 97.1°C, 96.1°C, 95.1°C, 94.1°C, 93.2°C, 92.2°C, 91.2°C, and 89.2°C, respectively. The corresponding Cole-Davidson plots are illustrated in Fig. 12. In the present complex, the magnitude of dielectric loss decreases with decrease in temperature. The relaxation frequency is observed to be 825 KHz at 98.1°C with ε'' value of 0.3888. The relaxation frequency shifted to 1050 KHz as the temperature is decreased to 89.2°C with ε'' value of 0.3453. Thus, the relaxation frequency in smectic C phase is inversely proportional to the temperature. The distribution parameter α has been calculated for each relaxation process. The magnitude of α increases with decrease in temperature. The value of distribution parameter α is 0.4711 at 98.1°C while it increased to 0.8027 at 89.2°C. From the above

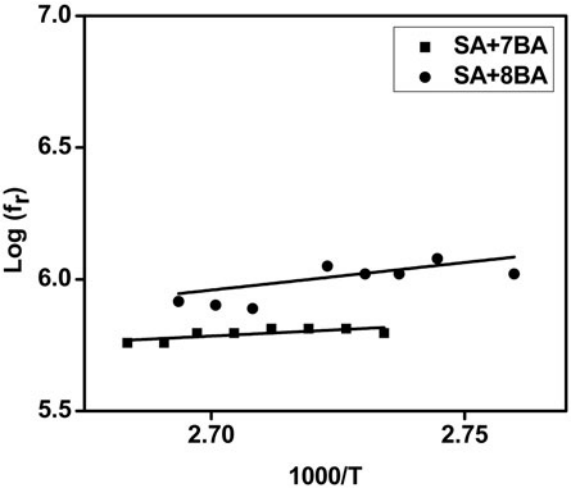

Figure 11. Arrhenius plot of SA + 7BA and SA + 8BA complexes.

data plots, Arrhenius plot (Fig. 11) is constructed and the activation energy is estimated to be 2.0988 eV. The values of relaxation frequency and corresponding temperature and activation energy are listed in Table 5.

3.8. Temperature Variation of Capacitance and Dielectric Loss

SA + 5BA complex of the present homologous series is taken as a representative case for this study and the variation of capacitance and dielectric loss with temperature are discussed. Simultaneous textural observations are also made to ascertain the phase of the mesogen and are co-related with the dielectric data. The readings of permittivity and dielectric loss are noted in the cooling run with a scan rate of 0.1°C. SA + 5BA complex filled in the

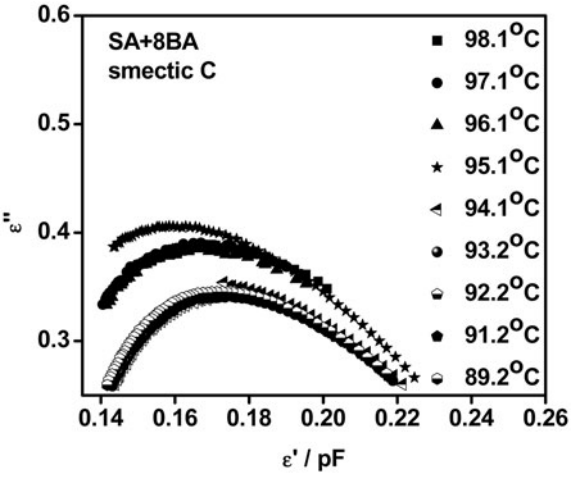

Figure 12. Dielectric dispersion curves in smectic C phase of SA + 8BA complex.

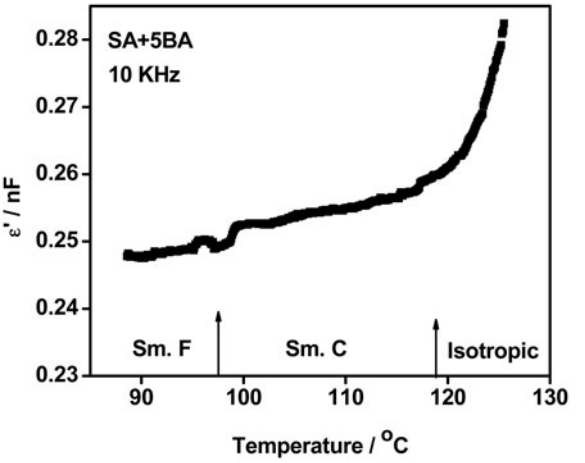

Figure 13. Temperature variation of capacitance at 10 KHz identifying various mesogens of SA + 5BA complex.

liquid crystal cell is provided with a sinusoidal stimulus of 1.1 volts derived from HP4192A impedance analyzer. The variation of the capacitance and dielectric loss at a frequency of 10 KHz are plotted in Figs. 13 and 14, respectively. The following points are noted from Figs. 13 and 14.

(1) In the isotropic state at 120°C, there is no anomaly in the variation of permittivity and dielectric loss.
(2) At the onset of smectic C phase at 119.1°C, a kink in the capacitance is observed that manifests the first-order transition from isotropic to smectic C phase. A similar trend of results is also evinced in the dielectric loss spectrum at 119.1°C.

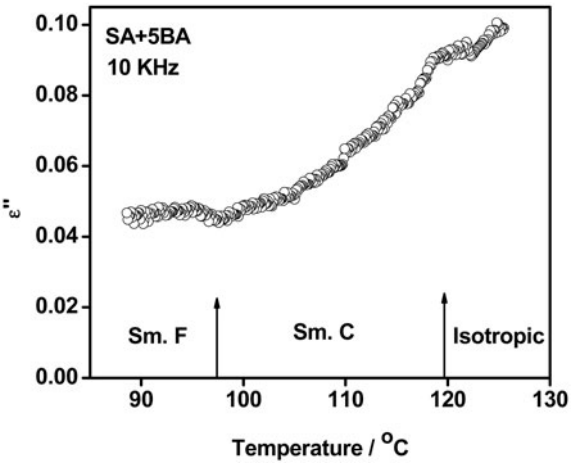

Figure 14. Temperature variation of dielectric loss at 10 KHz identifying various mesogens of SA + 5BA complex.

(3) Throughout the thermal range of smectic C (119.1°C–97.5°C), there is linear variation of the capacitance, which indicates the stabilization of smectic C phase. A similar trend of result is observed in dielectric loss spectrum.
(4) At 97.5°C, a kink in capacitance spectrum indicates the onset of smectic F phase. This being a first-order transition the anomaly in capacitance is pronounced. In the dielectric spectrum, a clear anomaly at 97.5°C is observed manifesting the phase transition from smectic C to smectic F.
(5) In the entire thermal range of smectic F, the magnitude of capacitance remained unaltered with temperature indicating the stabilization of smectic F phase. Similar result is observed in dielectric loss spectrum pertaining to smectic F phase.

3.9. Influence of Position of Oxygen atom

The inter hydrogen bonded complex of SA + *n*OBA are earlier reported [66] by us. The present homologous series of SA + *n*BA can be compared with SA + nOBA and following points can be inferred.

(1) The presence of oxygen enabled three phases, namely, nematic, smectic C, and smectic F, in all the eight complexes of SA + *n*OBA. In the present study, the phase diagram is composed of nematic, smectic C, smectic F, and smectic G phases. Thus, a new phase, smectic G, is induced in the present homologues series.
(2) The absence of oxygen in SA + *n*BA almost quenched nematic phase except for two homologues.
(3) The presence of oxygen enabled all the three phases (nematic, smectic C, and smectic F) to be present in all seven homologues of SA + *n*OBA while in SA + *n*BA, with the absence of oxygen, the phases are discrete in appearance except for smectic F.
(4) Thermal mesogenic range is observed to be enhanced with the presence of oxygen while the absence led to shrink the mesogenic range.
(5) Odd–even effect is pronounced in isotropic to nematic transition in SA + *n*OBA, while the absence of oxygen led to the annihilation of odd–even effect.
(6) Marginal improvements of tilt angle in smectic C are observed in the absence of oxygen atom.
(7) The presence of electro negative oxygen atom enabled for the formation of tri-variant phases (nematic, smectic C, and smectic F) in all the complexes of SA + *n*OBA while SA + BA exhibit mono, di-, and tri-variant phases.

4. Conclusions

(1) A novel series of HBLC homologous series is designed, synthesized, and characterized.
(2) The thermal stability factor for various phases in SA + *n*BA series has been estimated.
(3) Order of the phase transition of mesogenic phases has been determined by DSC and correlated with Novard and Cox ratio.
(4) Optical tilt angle is measured with respect to temperature in the smectic C phase and the values obtained are fitted to a power law equation. The critical exponent value of the power law is in concurrence with the mean field theory predicted value.

(5) Dielectric relaxation frequencies for different complexes in smectic phase are elucidated and the corresponding activation energy is determined.

Acknowledgments

The divine and graceful blessings of almighty Bannari Amman, the infrastructural support rendered by Bannari Amman Institute of Technology, and the financial support rendered by the Board of Research in Nuclear Sciences (BRNS) of Department of Atomic Energy (DAE), India (Sanction No. 2012/34/35/BRNS), are gratefully acknowledged by the authors.

References

[1] Paleos, C. M., & Siourvas, D. T. (2001). *Liq. Cryst.*, *28*, 1127.
[2] Sideratou, Z., Paleos, C. M., & Skoulios, A. (1995). *Mol. Cryst. Liq. Cryst.*, *265*, 19.
[3] Andersson, G., Dhal, W., Kuczynski, I., Lagerwall, S. T., Skarp, K., & Stebler, B. (1988). *Ferroelectrics*, *84*, 285.
[4] Wang, J. M., Kim, Y. J., Kim, C. J., & Kim, K. S. (2002). *Ferroelectrics*, *277*, 185.
[5] Aira, H., Ray, H., & Kohki, T. (2004). *Jpn. J. Appl. Phys.*, *43*, 6243.
[6] Wu, S. L., & Lin, C. Y. (2003). *Liq. Cryst.*, *30*, 205.
[7] Kato, T., Fukumasa, M., & Frechet, J. M. J. (1995). *Chem. Mater.*, *7*, 368.
[8] Niori, T., Sekine, T., Watanabe, J., Furukawa, J., Choi, S. W., & Takezoe, H. (1996). *J. Mater. Chem.*, *6*, 1307.
[9] Adams, H., Braily, N., Bruce, D. W., Dhillon, R., Dunmur, D. A., Hunt, S. E., Lalinde, E., Maggs, A. A., Orr, R., Styring, P., Wragg, M. S., & Maitlies, P. M. (1988). *Polyhedron*, *7*, 1861.
[10] Mikhaleva, M. A., Kolesnichenko, G. A., Rubina, K. I., Goldberg, Yu. Sh., Shimanskaya, M. V., & Mamaev, V. P. (1986). *Chem. Hetro. Compd.*, *22*, 310.
[11] Noot, C., Perkins, S. P., & Coles, H. J. (2000). *Ferroelectrics*, *244*, 331.
[12] Cook, A. G., Baumeister, U., & Tschierske, C. (2005). *J. Mater. Chem.*, *15*, 1708.
[13] Brienne, M. J., Gabard, J., Lehn, J. M., & Stibor, J. (1989). *J. Chem. Soc. Chem. Commun.*, *186*, 8.
[14] Kato, T., Mizoshita, N., & Kanie, K. (2001). *Macromol. Rapid. Commun.*, *22*, 797.
[15] Kumar, S. (2011). *Chemistry of Discotic Liquid Crystals*, CRC Press: Boca Raton, FL.
[16] Lehn, J. M. (2002). *Science*, *295*, 2400.
[17] Prins, L. J., Reinhoudt, D. N., & Timmerman, P. (2001). *Angew. Chem.*, *113*, 2446.
[18] Kato, T., & Frechet, J. M. J. (1989). *J. Am. Chem. Soc.*, *111*, 8533.
[19] Kato, T. (2000). *Hydrogen Bonded Liquid Crystals*, Springer: Heidelberg.
[20] Kihara, H., Kato, T., Uryu, T., Ujiie, S., Kumar, U., Frechet, J. M. J., Bruce, D. W., & Price, J. D. (1996). *Liq. Cryst.*, *21*, 25.
[21] Parra, M., Hidalgo, P., & Alderete, J. (2005). *Liq. Cryst.*, *32*, 449.
[22] Brand, H. R., Cladis, P. E., & Pleiner, H. (1992). *Macro. Mol.*, *25*, 7223.
[23] Goodby, J. W. (1991). *Ferroelectric Liquid Crystals: Principles, Properties, and Applications*, Gordon & Breach: Philadelphia, PA.
[24] de Gennes, P. G. (1974). *The Physics of Liquid Crystals*, Oxford University Press: Oxford.
[25] Kavitha, C., & Madhu Mohan, M. L. N. (2012). *J. Phys. Chem. Solids*, *73*, 1203.
[26] Kavitha, C., Pongali Sathya Prabu, N., & Madhu Mohan, M. L. N. (2012). *Physica B*, *407*, 859.
[27] Pongali Sathya Prabu, N., & Madhu Mohan M. L. N. (2013). *J. Mol. Liq.*, *182*, 79.
[28] Kavitha, C., Pongali Sathya Prabu, N., & Madhu Mohan, M. L. N. (2012). *Phase Transitions*, *85*, 973.
[29] Kang, S. K., & Samulski, E. T. (2000). *Liq. Cryst.*, *27*(3), 371.
[30] Hentrich, F., Diele, S., & Tschierske, C. (1994). *Liq. Cryst.*, *17*, 827.
[31] Kobayashi, Y., & Mtsunage, Y. (1987). *Bull. Chem. Soc. Jpn.*, *60*, 3515.

[32] Kato, T., Kihara, H., Uryu, T., Fujishima, A., & Frechet, J. M. J. (1992). *Macromolecules*, *25*, 6836.
[33] Pongali Sathya Prabu, N., & Madhu Mohan, M. L. N. (2012). *Phase Transitions*, *86*, 339.
[34] Kato, T., & Frechet, J. M. J. (1989). *Macromolecules*, *22*, 3818.
[35] Kumar, U., Kato, T., Frechet, J. M. J., & Am, J. (1992). *Chem. Soc.*, *114*, 6630.
[36] Kumar, U., Frechet, J. M. J., Kato, T., Ujiie, S., & Iimura, K. (1992). *Angew. Chem. Int. Ed. Engl.*, *31*, 1531.
[37] Yu, L. J. (1993). *Liq. Cryst.*, *14*, 1303.
[38] Kato, T., Wilson, P. G., Fujishima, A., & Frechet, J. M. J. (1990). *Chem. Lett.*, *19*, 2003.
[39] Tian, Y. Q., Su, F. Y., Shao, Y. Y., Lu, X. Y., Tang, X. Y., Zhao, X. G., & Zhou, E. L. (1995). *Liq. Cryst.*, *19*, 743.
[40] Pongali Sathya Prabu, N., Vijayakumar, V. N., & Madhu Mohan, M. L. N. (2011). *J. Mol. Str.*, *1994*, 387.
[41] Pongali Sathya Prabu, N., Vijayakumar, V. N., & Madhu Mohan, M. L. N. (2011). *Physica B*, *406*, 1106.
[42] Pongali Sathya Prabu, N., Vijayakumar, V. N., & Madhu Mohan, M. L. N. (2011). *Mol. Cryst. Liq. Cryst.*, *548*, 142.
[43] Lehn, J. M. (1995). *Supramolecular Chemistry: Concepts and Perspectives*, VCH: Weinheim.
[44] Fouquey, C., Lehn, J. M., & Mlevelut, A. (1990). *Adv. Mater.*, *2*, 254.
[45] Pongali Sathya Prabu, N., & Madhu Mohan, M. L. N. (2012). *Mol. Cryst. Liq. Cryst.*, *569*, 72.
[46] Pongali Sathya Prabu, N., Potukuchi, D. M., & Madhu Mohan, M. L. N. (2012). *Physica B*, *407*, 3709.
[47] Navard, P., Cox, R. (1984). *Mol. Cryst. Liq. Cryst.*, *102*, 261.
[48] Pongali Sathya Prabu, N., & Madhu Mohan, M. L. N. (2012). *J. Therm. Anal. Cal.*, *113*, 811.
[49] Pongali Sathya Prabu, N., & Madhu Mohan, M. L. N. (2012). *Mol. Cryst. Liq. Cryst.*, *557*, 144.
[50] Gray, G. W., & Goodby, J. W. G. (1984). *Smectic Liquid Crystals: Textures and Structures*, Leonard Hill: London.
[51] Kato, T., Uryu, T., Kaneuchi, F., Jin, C., & Frechet, J. M. J. (1993). *Liq. Cryst.*, *14*, 1311.
[52] Pavia, D. L., Lampman, G. M., & Kriz, G. S. (2007). *Introduction to Spectroscopy*, Sanat Printers: Heidelberg.
[53] Nakamoto, K. (1978). *Infrared and Raman Spectra of Inorganic and Co-Ordination Compounds*, Wiley-Interscience: New York.
[54] Xu, J. (2006). *J. Mater. Chem.*, *16*, 3540.
[55] Frechet, J. M. J., & Kato, T. (1992). Patent US No. 5139696.
[56] Pongali Sathya Prabu, N., & Madhu Mohan, M. L. N. (2013). *Phase Transitions*, *86*(4), 339.
[57] Smith, G. W., & Gardlund, Z. G. (1973). *J. Chem. Phys.*, *59*(2), 3214.
[58] Osman, Z. (1976). *Naturforsh*, *31b*, 801.
[59] Chandrasekhar, S. (1977). *Liquid Crystals*, Cambridge University Press: New York.
[60] Vijayakumar, V. N., & Madhu Mohan, M. L. N. (2009). *Sol. State Commun.*, *149*, 2090.
[61] Sato, A., Kato, T., & Uryu, T. (1996). *J. Polym. Sci. A: Polym. Chem.*, *34*, 503.
[62] Stanley, H. E. (1971). *Introduction to Phase Transition and Critical Phenomena*, Clarendon Press: New York.
[63] Hills, N. E., Wanghan, W. E., Price, A. H., & Davies, M. (1969). *Dielectric Properties and Molecular Behavior*, Vannostrand: New York.
[64] Jonscher, A. H. (1983). *Dielectric Relaxation in Solids*, Chelsea Dielectric Press: London.
[65] Cole, R. H. (1941). *J. Chem. Phys.*, *9*, 341.
[66] Subhapriya, P., Vijayanand, P. S., & Madhu Mohan, M. L. N. (2013). *Mol. Cryst. Liq. Cryst.*, *571*, 40.